Materials Chemistry and Physics 209 (2018) 217–226

Contents lists available at ScienceDirect

Materials Chemistry and Physics

journal homepage: www.elsevier.com/locate/matchemphys

Influence of vinyl bonds from PDMS on the pore structure of polymer derived ceramics

Donald Erb, Kathy Lu*

Department of Materials Science and Engineering, Virginia Tech, Blacksburg, VA, 24061, USA

HIGHLIGHTS

- Precursor phase separation during crosslinking can create pores in ceramics.
- Contents of hydrogen and vinyl bonds influence final porosity and pore size.
- v-PDMS with vinyl bonds decreases pore size and narrows pore size distribution.
- Excess hydrogen bonds from the base polymer with v-PDMS eliminates porosity.

GRAPHICAL ABSTRACT

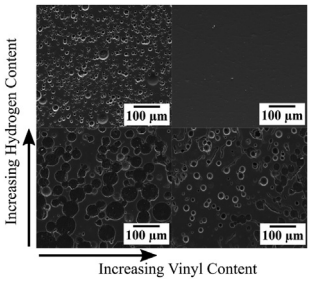

ARTICLE INFO

Article history:
Received 7 December 2017
Received in revised form
21 January 2018
Accepted 30 January 2018
Available online 3 February 2018

Keywords:
Silicon oxycarbide
Polymer-derived ceramics
Porosity
Phase separation
Vinyl bond

ABSTRACT

The influence of vinyl bonds on the phase separation and decomposition of polydimethylsiloxane (PDMS) was investigated for a saturated PDMS (s-PDMS) and an unsaturated poly(dimethylsiloxane-*co*-vinylmethylsiloxane) (v-PDMS) with the same molecular weight, and the resulting pore sizes were investigated for two base polymer systems, one with an excess of hydrogen bonds (PHMS, polyhydromethylsoloxane) and one with stoichiometric hydrogen to vinyl bonds (PSO, polysiloxane). For PHMS, the samples with s-PDMS have lower ceramic yield and higher total porosity, while the samples with v-PDMS contain nearly no porosity after pyrolysis to 1300 °C due to extensive hydrosilylation between the hydrogen and vinyl groups. For the PSO, both s-PDMS and v-PDMS produce micron-sized pores, but the v-PDMS produces smaller pores with a narrower size distribution than the s-PDMS. The fundamental differences in the polymer phase separation and decomposition arising from the addition of vinyl bonds to the PDMS chains and the effect of the base polymer hydrogen content are discussed.

1. Introduction

Porous ceramic components containing macro-, meso-, and/or micro-pores are important for applications such as catalyst supports, thermal insulation, and gas separation membranes [1]. The use of polymer derived ceramics offers distinct advantages over traditional powder based processing techniques due to lower processing temperatures and a wide range of available compositions [2,3]. In particular, porous silicon oxycarbide (SiOC) is an excellent candidate due to its resistance to chemical and oxidation degradation, high temperature stability, and excellent mechanical properties [1,2,4–6].

There are several routes to fabricate porous polymer derived ceramics, including sacrificial fillers [7–9], foaming [10–14], freeze casting [15,16], selective etching of a ceramic phase [17–22], and polymer phase decomposition [23–25]. The pore size, shape, and

* Corresponding author. 213 Holden Hall, Virginia Tech, Blacksburg, VA, 24061, USA.
E-mail address: klu@vt.edu (K. Lu).

https://doi.org/10.1016/j.matchemphys.2018.01.078
0254-0584/

distribution within polymer derived ceramics can be tailored to fit a specific application: pores created by selective etching or polymer decomposition are often spherical and uniformly distributed and are well suited for thermal insulation or adsorption of gas, ions, and dyes [22–25]; pores created using foaming or freeze casting can be directionally aligned and useful in applications requiring high permeability such as catalysis and filtration [10,15,16]. One particular processing strategy, polymer phase separation followed by selective decomposition of one of the polymers, such as polydimethylsiloxane (PDMS), during pyrolysis has gained attention in recent years as a convenient processing route to create porous SiOC and SiC ceramics with different pore sizes [3,23–25]. The pore sizes resulting from the decomposition of the PDMS phase can range from meso-to macro-scale depending on the processing conditions. The effects of various processing variables on the pore size and porosity have been researched, including the viscosity of the PDMS [26], the content of PDMS in the polymer blend [23–26], the base polymer system [3,23], and the pyrolysis temperature [24]. However, the studies thus far have been largely empirical, with the given results being specific to the polymer system used.

Recently, Blum et al. [24] reported the fabrication of mesoporous SiOC through the hydrosilylation reaction of vinyl terminated PDMS and a hydrogen containing base polymer. By simply changing the molecular weight of the PDMS additive from 9400 g/mol to 155000 g/mol, the resulting pore size from the PDMS decomposition can vary between 5 nm and 32 nm [24]. This processing technique has achieved pore sizes corresponding to the molecular size of the PDMS molecule within the SiOC ceramics. However, there are fundamental differences between the vinyl terminated PDMS used by Blum et al. [24] and a fully saturated PDMS polymer typically used to fabricate porous SiOC [3,25,26]. Thus, additional research into the use of vinyl-containing PDMS is needed in order to understand the effects of the vinyl bonds during the decomposition of the PDMS molecules.

In this study, two PDMS molecules are compared with the only difference being the presence of vinyl bonds along the backbone of one of the PDMS polymers (s-PDMS vs. v-PDMS). Further, two different base polymers are used, one with an excess of hydrogen bonds (PHMS) and the other with an equimolar amount of hydrogen and vinyl bonds (PSO), to illustrate the effect of the vinyl bonds during pyrolysis when either bonded during crosslinking through hydrosilylation or when left unsaturated.

2. Experimental procedures

Polyhydromethylsiloxane (PHMS, $M_W \sim 1600$ g/mol, $(CH_3)_3SiO[-Si(H)CH_3O-]_nSi(CH_3)_3$, Gelest Inc., Morrisville, PA) was chosen as the precursor for one of the base polymer systems used, and divinylbenzene (DVB, $M_W = 130.2$ g/mol, Sigma-Aldrich, St. Louis, MO) was used as the crosslinking agent. The other base polymer system used was a commercial polysiloxane (PSO, $[-Si(C_5H_6)_2O-]_3[-Si(CH_3)(H)O-]_2[-Si(CH_3)(CH{=}CH_2)O-]_2$, SPR-684, viscosity: 10 Pa s, Starfire Systems, Inc., Schenectady, NY). For both polymers, 2.1–2.4% platinum-divinyltetramethyldisiloxane complex in xylene (Pt catalyst, Gelest Inc., Morrisville, PA) was used as the catalyst. A fully saturated PDMS ($M_W = 28000$ g/mol, $(CH_3)_3SiO[-Si(CH_3)_2O-]_nSi(CH_3)_3$, viscosity: 1 Pa s, Fisher Scientific, Pittsburgh, PA) and a PDMS copolymer containing 7–8% vinylmethylsiloxane (VDT-781, $M_W = 28000$ g/mol, $(CH_3)_3SiO[-Si(CH_3)_2O-]_n[Si(CH_3)(CH{=}CH_2)O-]_m(Si(CH_3)_3$, viscosity: 0.8–1.2 Pa s, Gelest Inc., Morrisville, PA) were selected as the additives and pore forming species.

First, a mixture of PHMS and DVB with a 1:0.6 wt ratio was prepared, which was simply labelled as PHMS in this study for brevity; the PHMS mixture had a viscosity of 0.01 Pa s. Then PHMS-PDMS or PSO-PDMS mixtures containing 0, 10, 20, or 30 wt% of both types of PDMS were mixed. Toluene (Fisher Scientific, Pittsburgh, PA) was added to the PSO solutions as needed to provide a suitable viscosity for mixing. The solution was mixed for 15 min using a high energy mill (SPEX 8000 M Mixer/Mill, SPEX SamplePrep, Metuchen, NJ). Next, the Pt catalyst (5 ppm relative to PHMS, 225 ppm relative to PSO) was added, the mixture was milled again for 5 min and then poured into aluminum foil molds. The mixture was placed into a vacuum chamber and vacuumed to approximately 20 Torr for 30 min to remove any solvent or trapped bubbles. After that, the mixture was crosslinked in an oven at 50 °C for 12 h, 80 °C for 10 h, and then at 120 °C for 6 h. Samples are denoted as either PHMS-Xs or PSO-Xs for the samples containing saturated PDMS and PHMS-Xv or PSO-Xv for samples with the vinyl containing PDMS; X is the weight percent of PDMS in the polymer blend.

To prepare the samples for pyrolysis, the crosslinked polymers were first cut and polished into pieces roughly 10 mm in length and 2 mm in thickness. Next, the samples were placed into a zirconia crucible, covered on both sides with graphite mats in order to reduce friction during shrinkage and prevent warping [27,28], and put into a tube furnace (1730-20 Horizontal Tube Furnace, CM Furnaces Inc., Bloomfield, NJ). The samples were heated up to 1300 °C at a rate of 1 K/min, held for 2 h, cooled to 400 °C with a rate of 1 K/min, and finally cooled to 50 °C with a rate of 2 K/min, all with an Ar flow (500 std cm^3/min). When the furnace was between 500 and 700 °C during heating, the Ar was bubbled through water at 60 °C, giving a gas flow with a Ar:H_2O molar ratio of approximately 5:1. The 500°C-700 °C water vapor injection was used to facilitate SiO_2 formation, and the temperature range was chosen because it corresponded to the temperature range at which most mass loss occurs for the base polymers.

Etching of the bulk SiOC samples after pyrolysis was done using a solution of HF (20 wt% HF in water). The HF solution was magnetically stirred at room temperature until the SiOC samples had no significant mass loss, taking approximately 3 days. The SiOC samples were then rinsed with deionized water and dried at 120 °C. The mass loss due to etching was calculated by dividing the change in mass after etching by the original mass.

The chemical bonding was evaluated using Fourier Transform Infrared Spectroscopy (FT-IR) (Nicolet 8700 with Pike GladiATR attachment, Thermo Scientific, Waltham, MA), which recorded between 500 and 4000 cm^{-1} wavenumber with a resolution of 4 cm^{-1} and averaged between 64 scans. The thermal decomposition of the polymers was investigated by thermogravimetric analysis (TGA) using a STA 449C Jupiter® analyzer (Netzsch-Gerätebau GmbH, Selb, Germany) with a temperature range of room temperature to 1000 °C, a heating rate of 5 °C/min, and a N_2 flux of 40 ml/min. Linear shrinkage and ceramic yield were calculated by measuring the dimensions and mass, respectively, of the samples before and after the pyrolysis; bulk density and apparent density were calculated using the Archimedes method with water as the medium. An environmental SEM (Quanta 600 FEG, FEI, Hillsboro, OR) was used to observe the microstructures of the pyrolyzed samples. Pore size distributions were obtained from high contrast SEM images, with three images per sample, using the image analysis software ImageJ [29]. The specific surface area and pore volume of micro-/meso-pores within the samples after the HF etching was measured using nitrogen adsorption at 77 K (NOVA 2200e, Quantachrome Instruments, Boynton Beach, FL). The viscosity of the polymers was measured at room temperature with a rheometer (AR 2000, TA Instruments, New Castle DE) and a cone-plate geometry.

3. Results and discussion

3.1. Polymer chemical structure

The PHMS-PDMS solutions after mixing but before crosslinking were transparent for both the v-PDMS and s-PDMS samples. After crosslinking, however, the s-PDMS samples became opaque while the v-PDMS samples remained transparent, as shown in Fig. 2(a). The opaque appearance of the s-PDMS samples is due to phase separation of the PDMS molecules from the PHMS because the two polymers have little to no crosslinks (Fig. 2(c)), and significant scattering of light occurs as the phase boundary grows to several hundred nanometers or greater, the same scale as the wavelength of visible light. The opaque nature of the PHMS-PDMS crosslinked system has also been observed in other studies using PDMS [25]. For the v-PDMS samples, however, the samples remain transparent, similar to the pure PHMS sample, up to 30 wt% v-PDMS. The hydrosilylation (Fig. 1) reaction between the hydrogen bonds in the PHMS and the vinyl bonds in the v-PDMS [24,30,31] may have prevented such large scale phase separation, leaving the sample transparent, as shown in Fig. 2(c). On the contrary, the PSO-PDMS solutions become opaque during mixing due to the incompatibility between PDMS and phenyl groups [32,33], and the polymer blends remain opaque after crosslinking for both the s-PDMS and v-PDMS polymers as shown in Fig. 2(b).

In addition to becoming opaque after crosslinking, the PHMS/s-PDMS samples also show different microstructures depending on the PDMS content. The PHMS-10s and PHMS-20s samples are composed of the PHMS matrix with the s-PDMS phase dispersed throughout with a close-to-spherical shape; the size of the s-PDMS phase increases as the weight percent of PDMS is increased from 10 wt% to 20 wt%. For the PHMS-30s sample, phase inversion has occurred, with the s-PDMS phase now comprising the matrix and the PHMS in a droplet form (Fig. 2(c)). This phase inversion behavior for blends of PHMS and s-PDMS was also observed by Yan et al. [25], which used tetramethyltetravinylcycletetrasiloxane as the crosslinking agent as opposed to DVB in this study. Due to the initial compatibility between the PHMS and PDMS molecules, the change in microstructure can be attributed to the crosslinking of the PHMS and DVB, which effectively increases the molecular weight of the PHMS until the PHMS and PDMS can no longer form a single phase and thus phase separate. This behavior is typical for systems that experience polymerization induced phase separation [34,35].

The FT-IR spectra for the crosslinked PHMS-PDMS polymers as well as the pure s-PDMS and v-PDMS polymers are shown in Fig. 3; each of the spectra is normalized to the Si-*O*-Si peak at ~1000 cm^{-1} in order to show differences between the samples. In the pure PHMS sample, the major absorption peaks are attributed to Si-*O*-Si (1000-1100 cm^{-1}), Si-CH_3 (1256 cm^{-1}), Si-H (2157 cm^{-1}), and CH_x (2868-2960 cm^{-1}). With the addition of s-PDMS, no new peaks are formed because the s-PDMS has no new chemical bonds compared to the PHMS. Between 20 wt% and 30 wt% s-PDMS, the absorbance peak due to Si-H disappears, which is attributed to the phase inversion behavior of the 30 wt% s-PDMS sample as already discussed. Since the PDMS phase surrounds the PHMS phase, the signal from the attenuated total reflectance (ATR) cannot penetrate through the PDMS phase, and the signal from the PHMS is not observable. Similar to the s-PDMS samples, the addition of v-PDMS causes no new peaks to form. However, the samples do not show the disappearance of the Si-H peak due to the more homogenous distribution of the polymers.

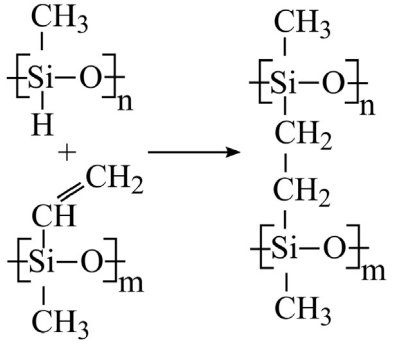

Fig. 1. Hydrosilylation reaction between hydrogen and vinyl bonds to induce crosslinks.

The FT-IR plots for the PSO-PDMS blends (Fig. 4) show no major differences in the spectra of the polymers after crosslinking. The spectra for both the s-PDMS in Fig. 4(a) and v-PDMS in Fig. 4(b) show similar peaks, which is to be expected since the vinyl content in the v-PDMS polymer is only 7–8 mol%. The PSO polymer has equal molar amounts of hydrogen and vinyl bonds, so the concentration of hydrogen bonds after crosslinking is minimal. Thus, the PSO polymer does not have an excess of Si-H bonds like the PHMS polymer. Due to this deficiency in Si-H bonds compared to vinyl bonds with the addition of v-PDMS, the probability of v-PDMS molecules attaching to the PSO through hydrosilylation is much less likely than for the PHMS base. The consumption of the hydrogen bonds in the PSO does not necessarily mean that the hydrogen bonds have all reacted with the vinyl bonds in the PSO rather than the v-PDMS polymer. However, given that the PSO and PDMS molecules readily phase separate due to the phenyl group in the PSO [33], the interaction between the PSO and PDMS molecules is likely much lower than the PSO molecules within the PSO phase.

3.2. Thermophysical properties

The decomposition behaviors of the base polymers, and the base polymers with 20 wt% addition of s-PDMS and v-PDMS are investigated using TGA, and the resulting TG and dTG curves are shown in Fig. 5. For the PHMS base polymers, the onset of decomposition for the PHMS-20s sample is at ~350 °C, while the PHMS and PHMS-20v samples begin decomposition at a slightly higher temperature of 400 °C. Initial degradation of trimethylsilylated PDMS is caused by the depolymerization of linear chains with the formation of cyclic siloxane products [36]. This depolymerization can be inhibited through increasing the crosslink density of the polymer, enhancing its thermal stability [36,37]. Thus, the higher onset degradation temperature for the PHMS and PHMS-20v samples can be attributed to a higher crosslinking density compared to that of the PHMS-20s sample. Both the PHMS and PHMS-20v samples have a maximum mass loss rate around 575 °C on the dTG curve and a second smaller maximum at 700 °C. After the completion of pyrolysis at 1000 °C, the PHMS and PHMS-20v samples have ceramic yields close to 80%, while the ceramic yield of the PHMS-20s sample is much lower at 64%. These differences in the decomposition behavior between the s-PDMS and v-PDMS samples can be attributed to the vinyl groups in the v-PDMS which promote the formation of Si-CH_2-Si or Si-CH_2-CH_2-Si bonds during pyrolysis and delay the decomposition of the PDMS molecules until much higher temperatures.

The decomposition behaviors of the PSO, PSO-20s, and PSO-20v samples are shown in Fig. 5(b). All three of the samples show two maxima on the dTG curves: one maximum at around 400 °C and the other around 550 °C. The PSO-20s sample shows a higher decomposition rate at 400 °C and has about the same decomposition rate as the PSO at 550 °C. Most likely, the mass loss centered at

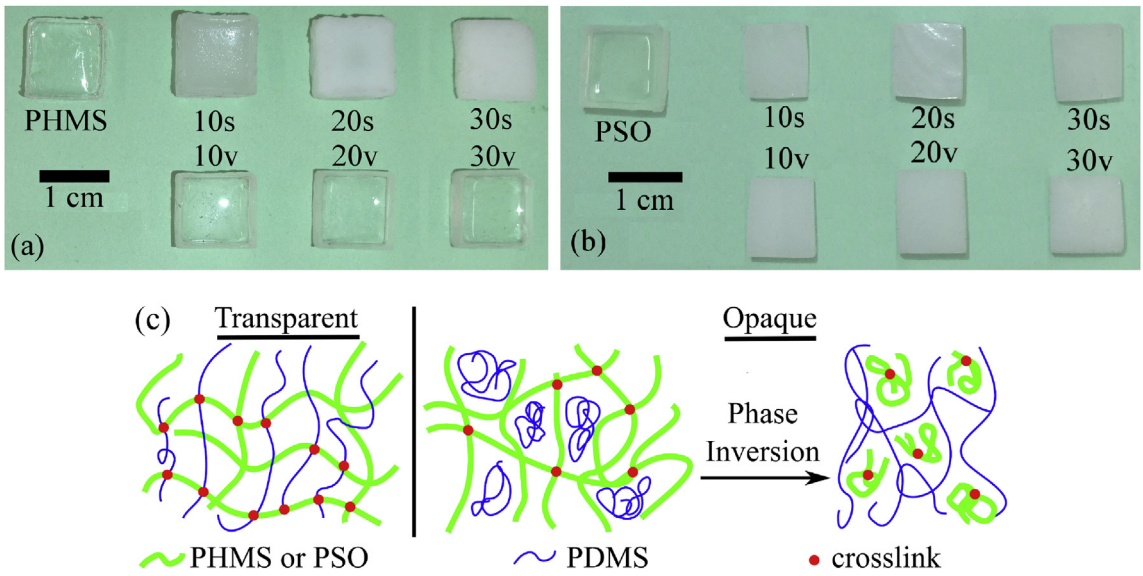

Fig. 2. Crosslinked samples for (a) PHMS base polymer and (b) PSO base polymer; (c) crosslinking difference between transparent and opaque samples.

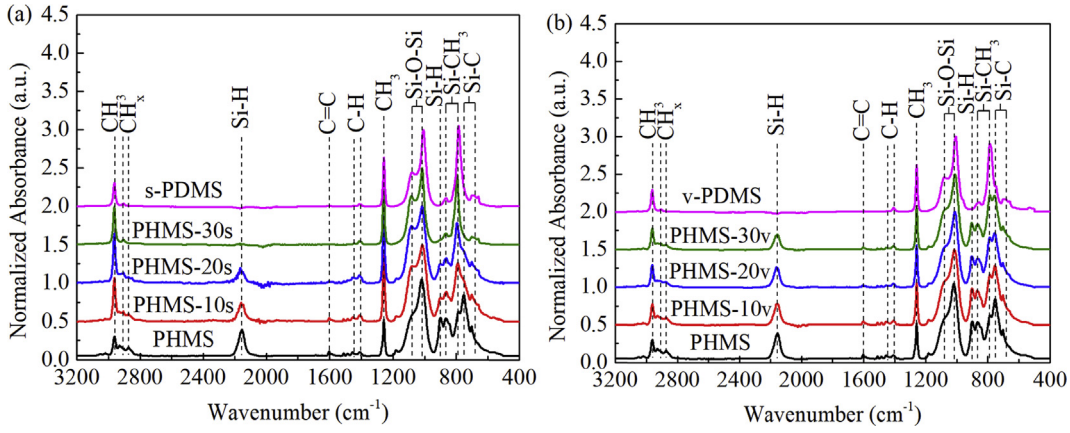

Fig. 3. FT-IR spectra for pure PHMS, 10–30 wt% PDMS, and pure PDMS: (a) s-PDMS, and (b) v-PDMS.

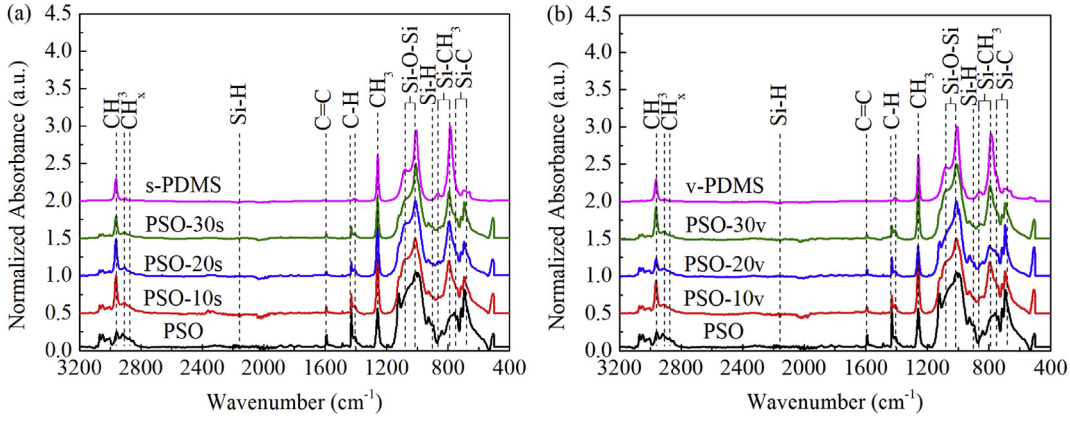

Fig. 4. FT-IR spectra for pure PSO, 10–30 wt% PDMS, and pure PDMS: (a) s-PDMS, and (b) v-PDMS.

400 °C is due to the decomposition of the PDMS molecules. The PSO-20v polymer has a similar decomposition rate as PSO at 400 °C, but then a much higher mass loss rate at 550 °C. The difference between the two types of PDMS molecules can again be attributed to the vinyl bonds in the v-PDMS sample. Even without forming Si-CH_2-CH_2-Si bonds through hydrosilylation, the vinyl groups can form additional bonds during pyrolysis, leading to strengthening of the polymer network [38]. Due to these additional bonds, the PSO-

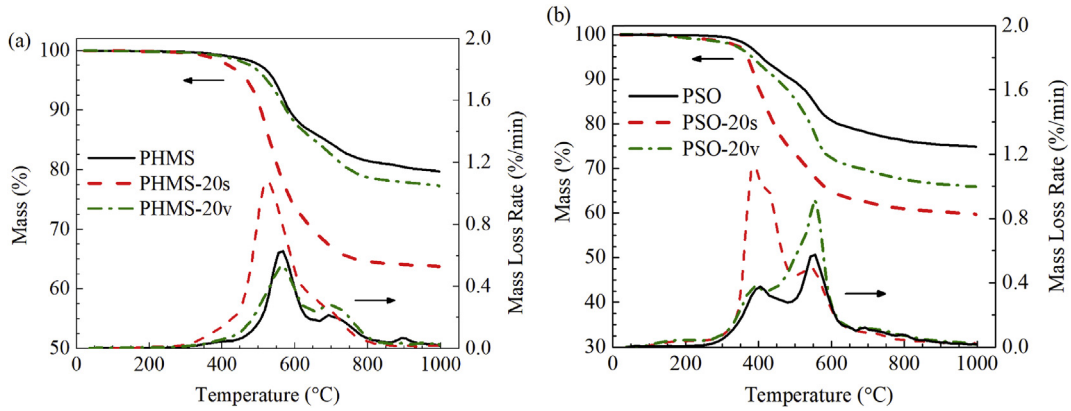

Fig. 5. TG and dTG of the (a) PHMS, PHMS-20s, PHMS-20v, and (b) PSO, PSO-20s, PSO-20v samples.

20v polymer has a slightly higher yield and a slower decomposition rate compared to the PSO-20s polymer; however, both polymers show much lower yields than the base PSO.

The ceramic yield and the linear shrinkage of the samples after pyrolysis at 1300 °C are given in Fig. 6. Compared to PHMS, the s-PDMS samples all have lower ceramic yields, as expected due to the decomposition of the PDMS molecules. With further addition of s-PDMS, the ceramic yield continues to decrease. For the v-PDMS samples, the ceramic yield for the 10 wt% v-PDMS sample is similar to that of the 10 wt% s-PDMS sample. However, for higher v-PDMS contents, the yield decreases only slightly, due to the vinyl bonds in the v-PDMS creating additional crosslinks and preventing the decomposition of all the PDMS molecules.

For the PSO base, the addition of s-PDMS decreases the ceramic yield for all the PDMS contents tested, confirming the decomposition of the PDMS molecules. With only 10 wt% v-PDMS, the ceramic yield of the PSO-PDMS polymer is increased. As the v-PDMS content is increased, however, the ceramic yield quickly decreases to a similar value to that of the s-PDMS samples. The change in the ceramic yield with the v-PDMS content can be attributed to the interaction between the PSO and v-PDMS polymers. With higher v-PDMS concentrations in the polymer mixture, the interactions between the PSO and v-PDMS molecules decrease, reducing the probability of interaction between the vinyl bonds in the v-PDMS and the hydrogen bonds in the PSO so that the phase separation of the two polymers occurs more readily. This would cause the v-PDMS sample to respond more similarly to the s-PDMS, which has no interaction with the PSO polymer, as clearly shown by the ceramic yield values in Fig. 6(b).

The linear shrinkage of the 10 wt% and 20 wt% s-PDMS samples decreases only slightly compared to that of the PHMS sample; with the addition of 30 wt% s-PDMS, the shrinkage increases much more, most likely due to the different microstructure of the 30 s-PDMS sample (Fig. 6(a)). For the v-PDMS samples, the linear shrinkage continually increases with the PDMS concentration. This behavior can be attributed to the sintering of the pores created from the v-PDMS, due to their much smaller size as to be discussed. The PSO samples show much less difference between the s-PDMS and v-PDMS samples, since there is little to no hydrosilylation occurring between the PSO and v-PDMS polymers (Fig. 6(b)). Further, the linear shrinkage also shows no dependence on the content of PDMS within the polymer, with all PSO/PDMS samples showing linear shrinkage values close to that of the pure PSO sample.

3.3. Porosity and pore size

The bulk and apparent densities for the PHMS/PDMS and PSO/PDMS samples are shown in Table 1. The bulk density takes into account the volume of the SiOC matrix and the open and closed pores; the apparent density considers the volume of the SiOC matrix and closed pores only. For the PHMS base, the samples with s-PDMS show a continual decrease in the bulk density while maintaining similar apparent densities. This result indicates that the open porosity of the PHMS/s-PDMS samples increases with increasing s-PDMS content while the closed porosity stays relatively constant. For the PHMS samples with v-PDMS, the bulk density shows no such dependence on the v-PDMS concentration, and all v-PDMS samples have similar bulk and apparent densities to

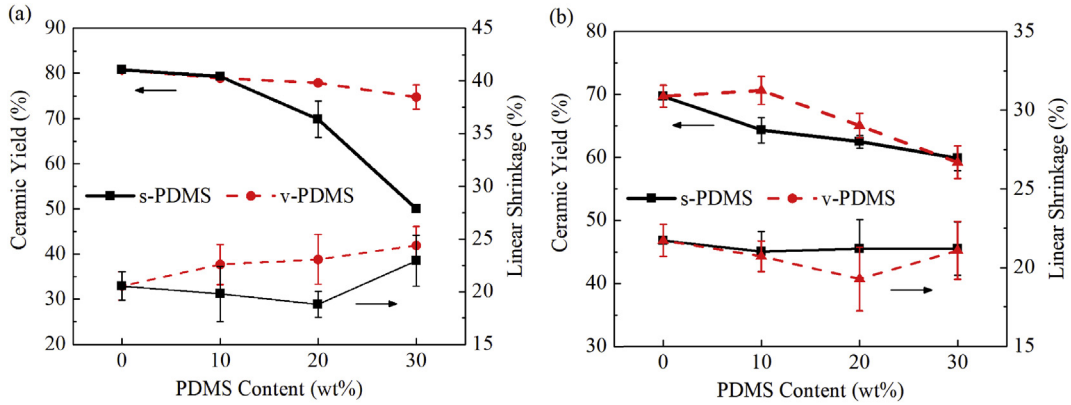

Fig. 6. Ceramic yield and linear shrinkage of the (a) PHMS and (b) PSO samples after pyrolysis at 1300 °C.

Table 1
Bulk and apparent densities of the PHMS and PSO samples after pyrolysis.

Base Polymer	PDMS Content (wt%)	Bulk Density, ρ_b (g/cm^3)		Apparent Density, ρ_a (g/cm^3)	
		s-PDMS	v-PDMS	s-PDMS	v-PDMS
PHMS	0	1.90 ± 0.05		2.01 ± 0.05	
PHMS	10	1.73 ± 0.02	1.90 ± 0.02	1.90 ± 0.02	2.01 ± 0.02
PHMS	20	1.65 ± 0.01	1.98 ± 0.05	1.84 ± 0.01	2.05 ± 0.05
PHMS	30	1.20 ± 0.02	1.90 ± 0.03	1.96 ± 0.01	2.05 ± 0.03
PSO	0	1.76 ± 0.01		1.88 ± 0.01	
PSO	10	1.59 ± 0.01	1.72 ± 0.01	1.77 ± 0.01	1.79 ± 0.01
PSO	20	1.51 ± 0.01	1.57 ± 0.01	1.83 ± 0.01	1.66 ± 0.01
PSO	30	1.44 ± 0.01	1.34 ± 0.01	1.79 ± 0.01	1.45 ± 0.01

the pure PHMS sample. This means that v-PDMS has no significant effect on the open porosity of the PHMS samples.

For the PSO/s-PDMS samples, the bulk densities decrease with increasing s-PDMS concentration while the apparent density remains relatively the same, again indicating that the open porosity is much more affected than the closed porosity by the s-PDMS samples. With the addition of v-PDMS to the PSO, both the bulk and apparent densities decrease, indicating that both the open and closed pore volumes increase with increasing v-PDMS content.

The density values listed in Table 1 can be used to compute the open porosity V_{op}, closed porosity V_{cp}, and total porosity V_{tp}, of the samples using the following equations:

$$V_{op} = 100(1\text{-}\rho_b/\rho_a) \quad (1)$$

$$V_{tp} = 100(1\text{-}\rho_b/\rho_t) \quad (2)$$

$$V_{cp} = V_{op} - V_{tp} \quad (3)$$

The true density for the samples with PDMS can be assumed to be equal to the measured apparent density of the base samples without PDMS because the majority of the PDMS should decompose and not affect the true density of the remaining ceramic; thus, the true density is estimated to be 2.01 g/cm^3 for all of the PHMS samples and 1.88 g/cm^3 for all of the PSO samples. Fig. 7 shows the results after applying Eqs. (1)–(3) to the density values in Table 1. For the pyrolyzed PSO and PHMS samples, the calculated total porosity is ~5%, which is most likely due to the cracks on the sample surface. With the addition of s-PDMS to PHMS (Fig. 7(a)), the porosity increases to 18% for the 20s-PDMS sample. The total porosity then increases greatly to 40% for the 30s-PDMS sample due to the phase inversion as previously discussed. Comparatively, the PHMS/v-PDMS samples show no significant change in porosity for the 10–30 wt% v-PDMS samples. This result indicates that all the pores created by the v-PDMS decomposition have closed during pyrolysis. It should be noted that both the open porosity and total porosity for the PHMS samples with v-PDMS overlap in Fig. 7(a) due to the absence of closed porosity within the samples.

For the PSO samples, the s-PDMS and v-PDMS polymers show distinct differences in open and total porosity trends (Fig. 7(b)). Addition of s-PDMS to the PSO matrix causes a continual increase in open porosity and total porosity, with the PSO-30s sample containing 24% total porosity. The difference between the total porosity and open porosity is similar for the three s-PDMS samples, indicating that s-PDMS strongly affects open porosity while maintaining similar closed porosity, and there is minimal interaction between PSO and s-PDMS and most s-PDMS escapes and leads to open pores during the pyrolysis. For the v-PDMS samples, the total porosity for the 10 wt% v-PSO sample is similar to that of the pure PSO sample. Increasing the v-PDMS content to 20 or 30 wt% causes a sharp increase in the total porosity, likely due to the lower interaction between the vinyl bonds in the v-PDMS and the hydrogen bonds in the PSO as already discussed in Section 3.2. Interestingly, the v-PDMS polymer affects the closed porosity much more strongly than the open porosity, showing an opposite trend to the s-PDMS polymer.

Fig. 8 shows the cross sections of the PHMS-20s and PHMS-20v samples after pyrolysis (all other conditions are in Fig. S1). With 10 wt% s-PDMS addition, the sample shows uniform, featureless microstructures. With 20 wt% s-PDMS addition, the sample has much larger pores, with the size ranging from 5 to 30 μm and a few pores reaching ~50 μm. As already discussed, the 30 wt% s-PDMS sample shows an inversion of the microstructure, with the pyrolyzed PHMS phase being made of loosely bonded spheres; the

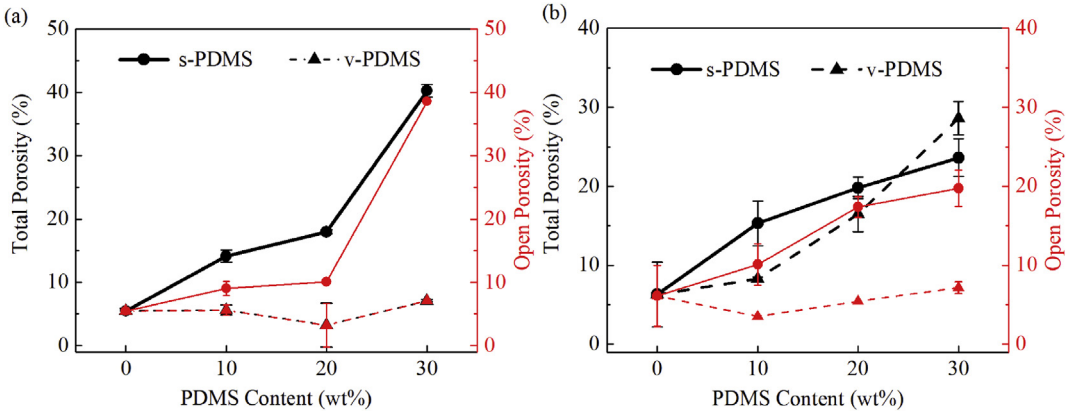

Fig. 7. Open and total porosities for (a) PHMS, and (b) PSO base polymers.

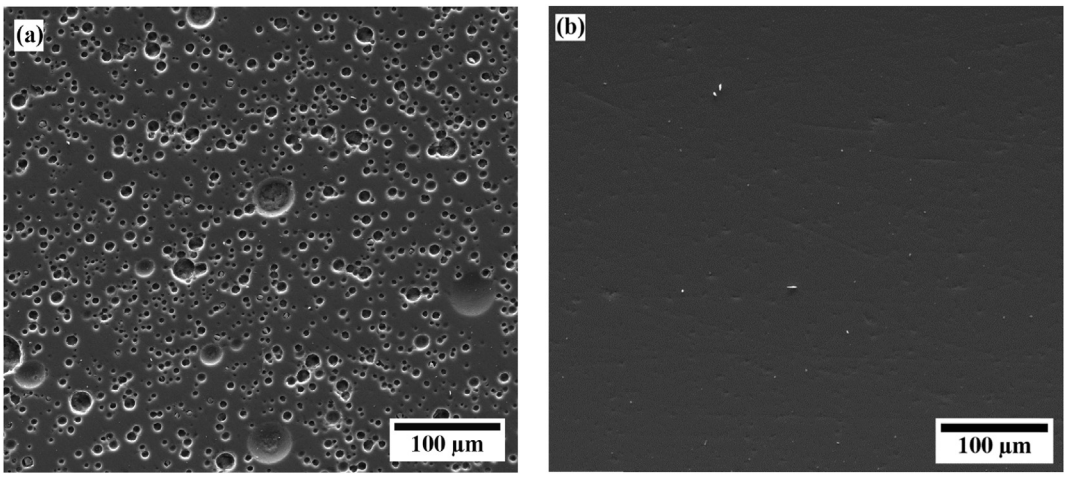

Fig. 8. SEM micrographs of pyrolyzed samples (a) PHMS-20s and (b) PHMS-20v.

spheres have a bimodal size with the smaller spheres reaching approximately 10 μm and the larger spheres having diameters of several hundred microns.

After pyrolysis, for the PHMS samples with v-PDMS, the pore size with 10 wt% addition shows a similar featureless microstructure as for the PHMS with 10 wt% s-PDMS sample (Fig. S1). However, the addition of higher amounts of v-PDMS does not show any significant changes to the microstructure (different from the corresponding s-PDMS samples), confirming the lack of porosity as measured with the Archimedes method. The reason for this observation with the v-PDMS samples can be understood by considering that the vinyl bonds within the v-PDMS sample react with the hydrogen bonds in the PHMS during crosslinking. Since the total molecular weight of the v-PDMS polymer is 28000 g/mol with 7–8 mol% vinylmethylsiloxane, then the average molecular weight of the PDMS chains between vinylmethylsiloxane molecules (or crosslinks) is approximately 900 g/mol, assuming that the vinylmethylsiloxane units are evenly distributed along the PDMS chains. For the PDMS polymers within the PHMS matrix, the conformation of the PDMS molecules can be assumed to be ideal; and the dependence of R_g for the PDMS molecules on the polymer molecular weight was determined by neutron scattering studies to be [39]:

$$R_g = 0.025M^{0.5}\ (\text{nm}) \tag{5}$$

The pore diameter left from the decomposition of PDMS molecules would simply be twice the value obtained from Eq. (5). Thus, if the average molecular weight between crosslinks for the v-PDMS molecules within the PHMS matrix is 900 g/mol, then the pore size would be approximately 1.5 nm following Eq. (5). Such small pores have been shown to easily close at higher temperatures, resulting in minimal porosity [24]. This hypothesis is further confirmed by considering the higher linear shrinkage of the v-PDMS samples in Fig. 6(a) versus the PHMS or PHMS-s samples.

To further examine whether microporosity may have arisen from the decomposition of the PDMS molecules, nitrogen adsorption was conducted on the pure PHMS and PSO samples as well as the samples with 20 wt% s-PDMS or v-PDMS, all after pyrolysis; the samples were first etched with a HF solution to remove SiO_2 from the samples and open the structure to allow for any closed pores from the PDMS decomposition to be available to the N_2 gas. The resulting pore size distributions for the samples (Fig. 9) show that no significant porosity can be observed other than that arising from the etching of the SiO_2 at ~1.6 nm and 3.5 nm. Thus, there is no significant residual microporosity from the decomposition of the s-PDMS and v-PDMS in either the PHMS or PSO.

The microstructures for the PSO-20s and PSO-20v mixtures after pyrolysis are shown in Fig. 10 (all the results for the other samples are shown in Fig. S1). The PSO-10s sample has a pore size range between 3 and 20 μm. The PSO-20s sample has a similar pore size range, with the only difference being the concentration of pores within the sample. An increase of the s-PDMS content to 30 wt% causes a much more drastic increase in the pore size to 20–50 μm, with a small concentration of pores still being 5–10 μm in diameter. Similar to the PSO-10s sample, the pore size for the PSO-10v sample is in the range of 3–20 μm (Fig. S1). With an increase of the v-PDMS content, both the pore size and pore size distribution increase, with the pore size ranging from 5 to 30 μm for both the PSO-20v and PSO-30v samples. This means that at higher concentrations of the v-PDMS, the pore formation more closely resembles that from the s-PDMS.

To further investigate the difference between the pore sizes for the PSO samples with s-PDMS and v-PDMS additions, the pore size distributions for the samples were obtained through image analysis of the SEM microstructures such as those shown in Fig. 10. The pore size measurements were not carried out for the PHMS samples due

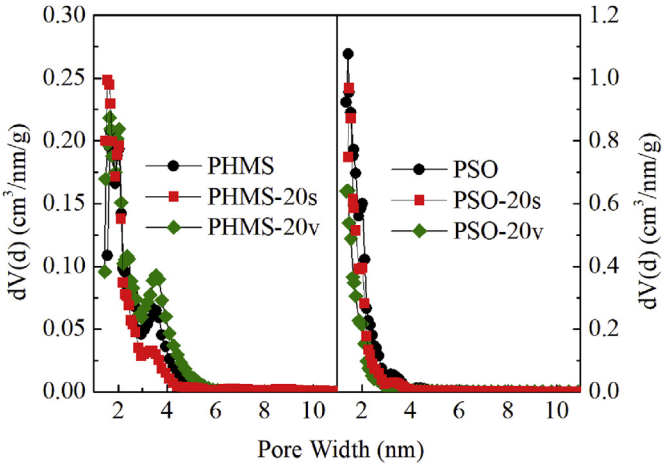

Fig. 9. Pore size distributions for the pure PHMS and PSO polymers after pyrolysis as well as the samples with 20 wt% PDMS additions.

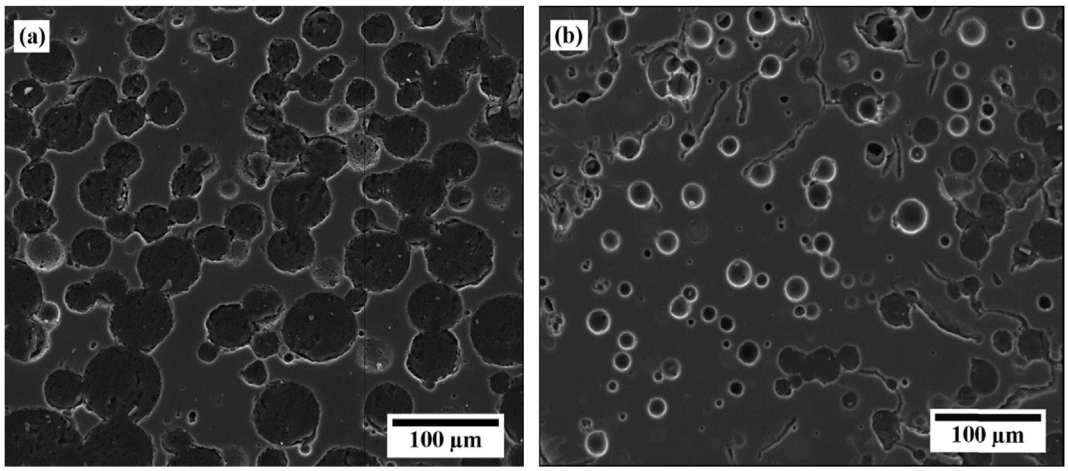

Fig. 10. SEM micrographs of pyrolyzed samples: (a) PSO-20s and (b) PSO-20v.

to the fact that only the PHMS-20s sample contains measureable porosity; the PHMS-10s and all of the PHMS-v samples contain negligible porosity, and the phase inversion for the PHMS-30s sample prevents any measurement of the PDMS phase. Fig. 11(a) and (b) show the area probability density, or the derivative of the cumulative pore area, for the PSO-PDMS samples. For the PSO-10s sample, the pore size distribution is wide and spans from 5 to 50 μm with a mode size of ~30 μm. Increasing the s-PDMS content to 20 wt% causes the pore size distribution to further widen, with the modes occurring at 35 μm and 65 μm. For the PSO-30s sample, the modes are at 20 μm, 50 μm, 75 μm, and 85 μm.

The pore size distributions for the PSO with v-PDMS in Fig. 11(b) all display narrower pore size distributions and smaller pore sizes than those for the s-PDMS samples. For the PSO-10v sample, the mode pore size is only 5 μm, and the sample contains no pores larger than 30 μm. Increasing the v-PDMS content to 20 wt% again

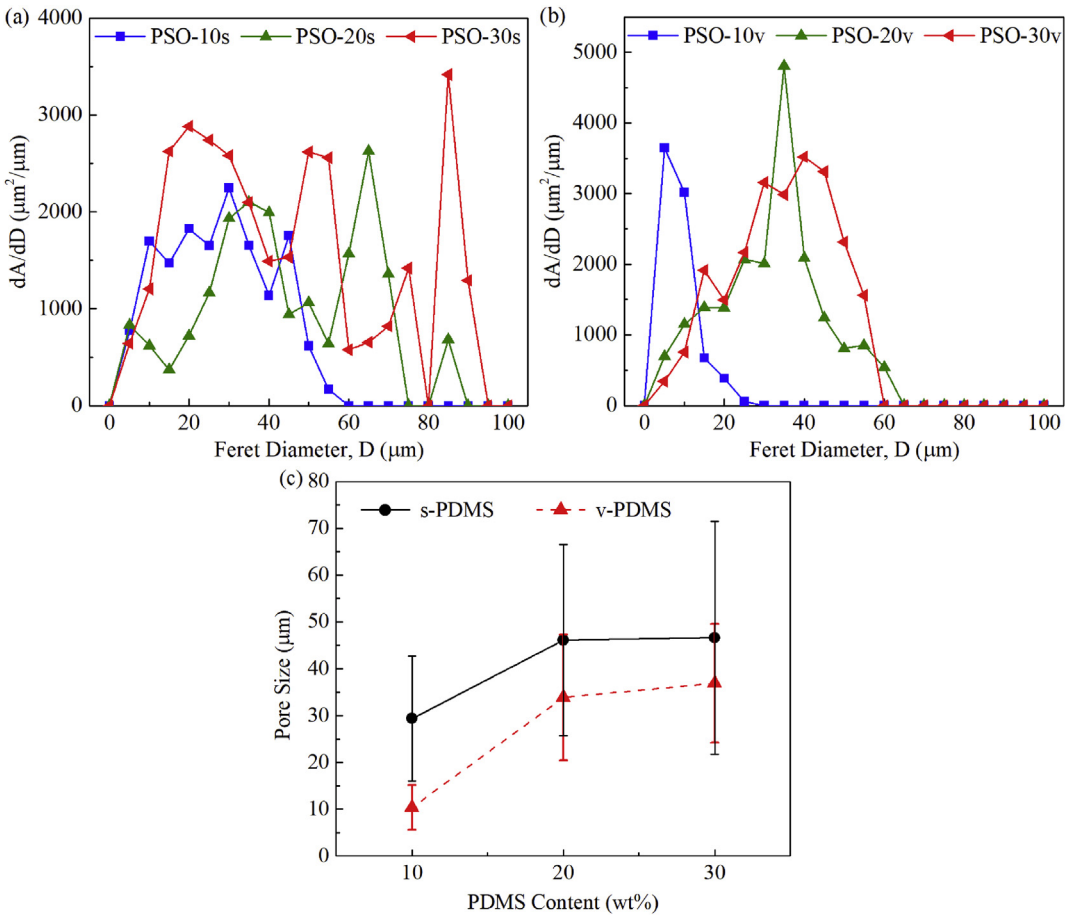

Fig. 11. Pore size distributions obtained from the SEM image analysis for PSO with: (a) s-PDMS, and (b) v-PDMS. (c) Average pore size for the PSO-s and PSO-v samples.

causes the pore size distribution to broaden and increases the mode pore size to 35 μm. The PSO-30v sample has a similar pore size distribution to the PSO-20v sample, with the mode pore size only increasing to 40 μm.

The average pore size and standard deviation for each of the PSO-PDMS samples are shown in Fig. 11(c). For the s-PDMS, the average pore size increases from 29.4 μm for the PSO-10s to 46.1 μm for the PSO-20s and then to 46.6 μm for the PSO-30s. The v-PDMS similarly increases with the PDMS content from 10.4 μm for the PSO-10v to 33.9 μm and 36.9 for the PSO-20v and PSO-30v, respectively. However, the standard deviations for the v-PDMS samples are much smaller than for the s-PDMS samples for each of the PDMS contents. The smaller pore sizes and narrower pore size distributions for the v-PDMS samples compared to the s-PDMS samples can only be attributed to the vinyl bonds within the v-PDMS, since both the molecular weight and the viscosity of the two types of PDMS are identical. As already seen from the TGA data in Fig. 5, the v-PDMS sample shows a different decomposition behavior than the s-PDMS sample due to the reactions from the vinyl group. Accordingly, these reactions may slightly prevent such extensive phase separation between the PSO and v-PDMS molecules. The reactions from the vinyl bonds along the v-PDMS chain may also effectively reduce the molecular weight of the PDMS molecules; the added connection points shorten the length of the free PDMS chains, reducing the PDMS molecular weight as already discussed for the PHMS/v-PDMS system. Both reducing the extent of phase separation and reducing the PDMS molecular weight would lead to smaller pore sizes and a narrower size distribution.

If the phase separation between the base polymer and the PDMS molecules is significant, as it is for the PSO base, then the size of the PDMS domains will be much larger than that of single polymer chains as discussed previously, given by Ref. [33]:

$$d = \frac{4\sigma_{int}(p+1)}{\dot{\gamma}\eta_m\left(\frac{19p}{4}+4\right)} \quad (6)$$

where p is the viscosity ratio of the dispersed phase to the matrix phase, σ_{int} is the interfacial tension of the two polymers, η_m is the viscosity of the matrix polymer, and $\dot{\gamma}$ is the sheer rate exerted on the system during mixing. If the polymer phases coalesce after mixing, then the polymer domains will increase in size according to the empirical relationship [33,40]:

$$d = \frac{4\sigma_{int}}{\dot{\gamma}\eta_m}(p)^{-0.84} \quad (7)$$

The measured viscosities of the PSO, s-PDMS, and v-PDMS are 10.7 ± 0.1 Pa s, 1.0 ± 0.1 Pa s, and 1.0 ± 0.1 Pa s, respectively. The interfacial tension is estimated to be ~0.00058 N/m, which is the value between PDMS and a poly(dimethylsiloxane-*ran*-methylphenylsiloxane), similar to the PSO used in this study [33]. Fig. 12 shows the result based on Eqs. (6) and (7) vs. the sheer rate during mixing as well as the average pore sizes. Considering that the sheer rate during the vibratory milling of the polymers is much greater than 1 1/s, then Eq. (7) more closely estimates the experimental pore sizes at a shear rate of approximately 40 1/s. Eq. (6) is based off the initial size of the polymer domains directly after mixing, while Eq. (7) takes into account coalescence of the domains after mixing, matching with the experimental results, since the PSO-PDMS mixtures were allowed to sit in the oven before reaching gelation.

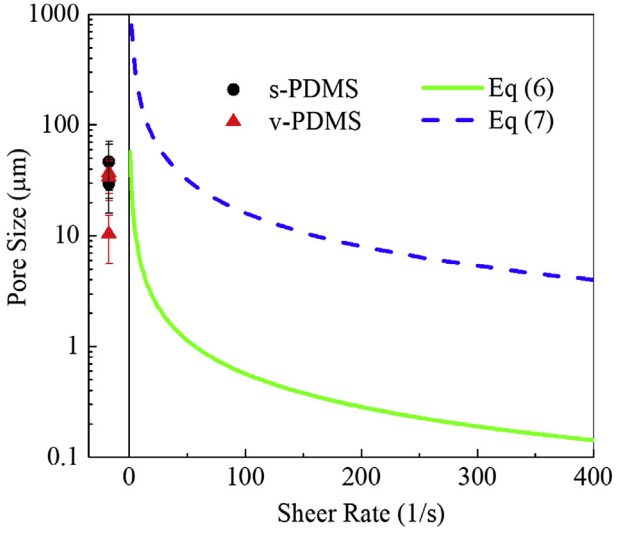

Fig. 12. Calculated pore size versus sheer rate during mixing from Eqs. (6) and (7), and the experimental pore sizes from Fig. 9(c).

4. Conclusions

Pores and porosity arising from the decomposition of PDMS have been studied for a fully saturated PDMS (s-PDMS) and a PDMS copolymer containing vinyl bonds (v-PDMS). The s-PDMS produces lower yields than the v-PDMS and higher porosity when added to PSO and PHMS base polymers, regardless of the content of hydrogen bonds in the base polymer. When crosslinked with the PHMS base, the v-PDMS does not show large scale phase separation, is more thermally stable than the s-PDMS, and produces no significant porosity. For low contents of v-PDMS crosslinked with the PSO base, the yield is higher and the porosity is lower compared to the corresponding s-PDMS samples, but the differences between the two PDMS types decreases as the PDMS content increases. For the PSO base containing no excess hydrogen bonds, the pores resulting from the PDMS decomposition are micron sized for both the s-PDMS and v-PDMS polymers. However, the PSO with v-PDMS produces smaller pores with a narrower pore size distribution than the s-PDMS, which is attributed to the vinyl bonds within the v-PDMS inducing reactions and effectively reducing the polymer molecular weight. The fundamental differences between the interaction of the PDMS molecules and the base polymers based on the vinyl content are discussed to provide a practical guide for polymer selection.

Acknowledgement

We acknowledge the financial support from National Science Foundation under grant number CMMI-1634325.

Appendix A. Supplementary data

Supplementary data related to this article can be found at https://doi.org/10.1016/j.matchemphys.2018.01.078.

Conflicts of interest

The authors declare that they have no conflict of interest.

References

[1] P. Colombo, Engineering porosity in polymer-derived ceramics, J. Eur. Ceram. Soc. 28 (2008) 1389–1395.
[2] P. Colombo, G. Mera, R. Riedel, G.D. Soraru, Polymer-derived ceramics: 40 years of research and innovation in advanced ceramics, J. Am. Ceram. Soc. 93

(2010) 1805–1837.
[3] Z.J. Yu, Y. Feng, S. Li, Y.X. Pei, Influence of the polymer-polymer miscibility on the formation of mesoporous SiC(O) ceramics for highly efficient adsorption of organic dyes, J. Eur. Ceram. Soc. 36 (2016) 3627–3635.
[4] G.D. Soraru, S. Modena, E. Guadagnino, P. Colombo, J. Egan, C. Pantano, Chemical durability of silicon oxycarbide glasses, J. Am. Ceram. Soc. 85 (2002) 1529–1536.
[5] K. Lu, D. Erb, M.Y. Liu, Thermal stability and electrical conductivity of carbon-enriched silicon oxycarbide, J. Mater. Chem. C 4 (2016) 1829–1837.
[6] K. Lu, D. Erb, M.Y. Liu, Phase transformation, oxidation stability, and electrical conductivity of TiO_2-polysiloxane derived ceramics, J. Mater. Sci. 51 (2016) 10166–10177.
[7] C. Vakifahmetoglu, D. Zeydanli, P. Colombo, Porous polymer derived ceramics, Mater. Sci. Eng. R 106 (2016) 1–30.
[8] J.M. Pan, X.H. Yan, X.N. Cheng, Q.B. Lu, M.S. Wang, C.H. Zhang, Preparation of SiC nanowires-filled cellular SiCO ceramics from polymeric precursor, Ceram. Int. 38 (2012) 6823–6829.
[9] B. Ceron-Nicolat, T. Fey, P. Greil, Processing of ceramic foams with hierarchical cell structure, Adv. Eng. Mater. 12 (2010) 884–892.
[10] C. Vakifahmetoglu, D. Zeydanli, M.D.D. Innocentini, F.D. Ribeiro, P.R.O. Lasso, G.D. Soraru, Gradient-hierarchic-aligned porosity SiOC ceramics, Sci. Rep. 7 (41049) (2017) 12.
[11] J. Zeschky, T. Hofner, C. Arnold, R. Weissmann, D. Bahloul-Hourlier, M. Scheffler, P. Greil, Polysilsesquioxane derived ceramic foams with gradient porosity, Acta Mater. 53 (2005) 927–937.
[12] S. Bhattacharjee, P.R. Das, C. Ohl, V. Wilker, M. Kappa, F. Scheffler, M. Scheffler, Novel-type inorganic foams from preceramic polymers with embedded titania nanoparticles for photo-catalytic applications, Adv. Eng. Mater. 13 (2011) 996–1001.
[13] C. Ohl, M. Kappa, V. Wilker, S. Bhattacharjee, F. Scheffler, M. Scheffler, Novel open-cellular glass foams for optical applications, J. Am. Ceram. Soc. 94 (2011) 436–441.
[14] G.W. Wen, H.W. Bai, X.X. Huang, Z.X. Han, Lotus-type porous SiOCN ceramic fabricated by undirectional solidification and pyrolysis, J. Am. Ceram. Soc. 94 (2011) 1309–1313.
[15] H.X. Zhang, C.L. Fidelis, M. Wilhelm, Z.P. Xie, K. Rezwan, Macro/mesoporous SiOC ceramics of anisotropic structure for cryogenic engineering, Mater. Design 134 (2017) 207–217.
[16] H.X. Zhang, C.L. Fidelis, A.L.T. Serva, M. Wilhelm, K. Rezwan, Water-based freeze casting: adjusting hydrophobic polymethylsiloxane for obtaining hierarchically ordered porous SiOC, J. Am. Ceram. Soc. 100 (2017) 1907–1918.
[17] L. Biasetto, R. Pena-Alonso, G.D. Soraru, P. Colombo, Etching of SiOC ceramic foams, Adv. Appl. Ceram 107 (2008) 106–110.
[18] R. Peña-Alonso, G.D. Sorarù, R. Raj, Preparation of ultrathin-walled carbon-based nanoporous structures by etching pseudo-amorphous silicon oxycarbide ceramics, J. Am. Ceram. Soc. 89 (2006) 2473–2480.
[19] J.K. Li, K. Lu, T.S. Lin, F.Y. Shen, Preparation of micro-/mesoporous SiOC bulk ceramics, J. Am. Ceram. Soc. 98 (2015) 1753–1761.
[20] J.K. Li, K. Lu, Highly porous SiOC bulk ceramics with water vapor assisted pyrolysis, J. Am. Ceram. Soc. 98 (2015) 2357–2365.
[21] D. Erb, K. Lu, Additive and pyrolysis atmosphere effects on polysiloxane-derived porous SiOC ceramics, J. Eur. Ceram. Soc. 37 (2017) 4547–4557.
[22] J. Yang, H.L. Wu, M. Zhu, W.J. Ren, Y. Lin, H.B. Chen, F. Pan, Optimized mesopores enabling enhanced rate performance in novel ultrahigh surface area meso-/microporous carbon for supercapacitors, Nano Energy 33 (2017) 453–461.
[23] C. Vakifahmetoglu, P. Colombo, A direct method for the fabrication of macroporous SiOC ceramics from preceramic polymers, Adv. Eng. Mater. 10 (2008) 256–259.
[24] Y. Blum, G.D. Soraru, A.P. Ramaswamy, D. Hui, S.M. Carturan, Controlled mesoporosity in SiOC via chemically bonded polymeric "spacers", J. Am. Ceram. Soc. 96 (2013) 2785–2792.
[25] X. Yan, D. Su, S.S. Han, Phase separation induced macroporous SiOC ceramics derived from polysiloxane, J. Eur. Ceram. Soc. 35 (2015) 443–450.
[26] J.Q. Wu, Y.M. Li, L.M. Chen, Z.B. Zhang, D. Wang, C.H. Xu, Simple fabrication of micro/nano-porous SiOC foam from polysiloxane, J. Mater. Chem. 22 (2012) 6542–6545.
[27] N. Janakiraman, F. Aldinger, Fabrication and characterization of fully dense Si-C-N ceramics from a poly (ureamethylvinyl) silazane precursor, J. Eur. Ceram. Soc. 29 (2009) 163–173.
[28] S. Martinez-Crespiera, E. Ionescu, H.J. Kleebe, R. Riedel, Pressureless synthesis of fully dense and crack-free SiOC bulk ceramics via photo-crosslinking and pyrolysis of a polysiloxane, J. Eur. Ceram. Soc. 31 (2011) 913–919.
[29] C.A. Schneider, W.S. Rasband, K.W. Eliceiri, NIH image to ImageJ: 25 years of image analysis, Nat. Methods 9 (2012) 671–675.
[30] D. Hourlier, S. Venkatachalam, M.R. Ammar, Y. Blum, Pyrolytic conversion of organopolysiloxanes, J. Anal. Appl. Pyrolysis 123 (2017) 296–306.
[31] S. Sakaki, N. Mizoe, M. Sugimoto, Theoretical study of platinum(0)-catalyzed hydrosilylation of ethylene. Chalk-harrod mechanism or modified chalk-harrod mechanism, Organometallics 17 (1998) 2510–2523.
[32] A. Stammer, B.A. Wolf, Effect of random copolymer additives on the interfacial tension between incompatible polymers, Macromol. Rapid Commun. 19 (1998) 123–126.
[33] V. Ziegler, B.A. Wolf, Viscosity and morphology of the two-phase system PDMS/P(DMS-ran-MPS), J. Rheol. 43 (1999) 1033–1045.
[34] H.M.J. Boots, J.G. Kloosterboer, C. Serbutoviez, F.J. Touwslager, Polymerization-induced phase separation. 1. Conversion-phase diagrams, Macromolecules 29 (1996) 7683–7689.
[35] C. Serbutoviez, J.G. Kloosterboer, H.M.J. Boots, F.J. Touwslager, Polymerization-induced phase separation. 2. Morphology of polymer-dispersed liquid crystal thin films, Macromolecules 29 (1996) 7690–7698.
[36] G. Camino, S.M. Lomakin, M. Lageard, Thermal polydimethylsiloxane degradation. Part 2. The degradation mechanisms, Polymer 43 (2002) 2011–2015.
[37] G. Camino, S.M. Lomakin, M. Lazzari, Polydimethylsiloxane thermal degradation - part 1. Kinetic aspects, Polymer 42 (2001) 2395–2402.
[38] A. Nyczyk-Malinowska, M. Wojcik-Bania, T. Gumula, M. Hasik, M. Cypryk, Z. Olejniczak, New precursors to SiCO ceramics derived from linear poly(-vinylsiloxanes) of regular chain composition, J. Eur. Ceram. Soc. 34 (2014) 889–902.
[39] N. Gilra, C. Cohen, R.M. Briber, B.J. Bauer, R.C. Hedden, A.Z. Panagiotopoulos, A SANS study of the conformational behavior of linear chains in compressed and uncompressed end-linked elastomers, Macromolecules 34 (2001) 7773–7782.
[40] S.H. Wu, Formation of dispersed phase in incompatible polymer blends - interfacial and rheological effects, Polym. Eng. Sci. 27 (1987) 335–343.